Stable Forbidden-Region Virtual Fixtures for Bilateral Telemanipulation

Jake J. Abbott[1]
e-mail: jabbott@ethz.ch

Allison M. Okamura
e-mail: aokamura@jhu.edu

Department of Mechanical Engineering,
Johns Hopkins University,
Baltimore, MD 21218

There has been recent interest in novel human-machine collaborative control laws, called "virtual fixtures," which provide operator assistance for telemanipulation tasks. A forbidden-region virtual fixture is a constraint, implemented in software, that seeks to prevent the slave manipulator of a master/slave telemanipulation system from entering into a forbidden region of the workspace. In this paper, we consider the problem of unstable vibrations of the slave and/or master against forbidden-region virtual fixtures for a general class of telemanipulator control architectures, including those with haptic feedback. To the best of the authors' knowledge, there has been no rigorous study of the stability of forbidden-region virtual fixtures in previous work. The system is evaluated around the master and slave equilibrium position resulting from a constant desired human input force, using a discrete state-space model. We present a method to analytically determine if instability is possible in the system. We thoroughly evaluate this method, experimentally, applying malicious user strategies that attempt to drive the system unstable. Our approach agrees with experimental results and can be used to design and analyze the stability and transient properties of a telemanipulator interacting with virtual fixtures. We show that the user can affect both slave- and master-side virtual fixture stability by modifying his or her impedance characteristics. However, the upper bound on stable slave-side virtual fixture stiffness does not depend on the particular user.
[DOI: 10.1115/1.2168163]

1 Introduction

Telemanipulation is the direct human control of a robotic manipulator, where the operator and the manipulator are at different locations. Telemanipulation can be used to accomplish a great number of tasks that are too remote, highly scaled, or hazardous for direct human manipulation. It is particularly advantageous in unstructured environments where completely autonomous robotic systems cannot be used due to the limitations of artificial intelligence, sensor-data interpretation, and environment modeling. Telemanipulation has current and potential benefits in diverse applications, such as space; undersea; hazardous nuclear, chemical, and biological environments; surgery; construction; mining; military; firefighting and lifesaving; warehousing; and entertainment [1].

"Bilateral" telemanipulation typically refers to a system where a human operator manipulates a master robotic device, and a slave device emulates the behavior of the master, with some form of haptic (force and/or tactile) feedback to the operator. Although haptic feedback can improve performance of telemanipulated tasks, traditional telemanipulation systems are not able to provide any intelligent assistance to the human operator. In addition, the accuracy and precision of even a perfectly designed telemanipulator is still ultimately limited by the accuracy and precision of the human user. Thus, we are developing novel human-machine collaborative control laws, called "virtual fixtures," which bridge the gap between strictly autonomous and strictly teleoperated systems. The term "virtual fixture" refers to a general class of guidance modes, implemented in software, that help a human-machine collaborative system perform a task by limiting movement into restricted regions and/or influencing movement along desired paths [2–12]. The potential benefit of virtual fixtures is safer and faster operation. Virtual fixtures attempt to capitalize on the accuracy of robotic systems, while maintaining a degree of operator control.

Virtual fixtures are particularly well suited for application in robot-assisted minimally invasive surgery (MIS). Telemanipulation has the potential to improve precision, dexterity, and visualization for the surgeon [13,14]. Bilateral telemanipulation systems can also decrease operation time and forces applied to the environment [15]. Virtual fixtures can further enhance robot-assisted MIS by ensuring that the remote manipulator does not enter forbidden areas of the workspace, such as organ surfaces (which should not be cut) or delicate tissue structures. We seek to develop virtual-fixture control laws that can be safely (stably) implemented on bilateral telemanipulators, with special consideration given to environments relevant to MIS tasks.

In this paper, we consider the stability of a particular type of virtual fixture, the forbidden-region virtual fixture (FRVF) [9], which prohibits the motion of a robot manipulator into a forbidden region of geometric or configuration space. A simple method of implementing FRVFs is with an impedance surface, or "virtual wall." This is a method commonly used in haptic interfaces for virtual environments, where the position (velocity, acceleration) of the device in relation to the impedance surface is used to generate an actuator force on the device. This paper is concerned with the implementation of these impedance-type FRVFs on telemanipulators where both the master and slave devices are of the impedance type (backdrivable, low mass).

The maximum stiffness of a virtual surface that can be implemented is limited by the sampling rate of the computer, the resolutions of the position sensor and actuator, and the impedance of the mechanical device [16]. Many researchers have investigated stability of virtual environments for haptic display; a review of these methods is given in [2,17]. Interaction with a haptic virtual environment through a proxy [18] is similar to bilateral telemanipulation, since the proxy serves as a slave manipulator that interacts with the virtual environment. However, analyzing

[1]Jake Abbott is now with the Institute of Robotics and Intellient Systems, ETH Zurich, CH-8092 Zurich, Switzerland.

Contributed by the Dynamic Systems, Measurement, and Control Division of ASME for publication in the JOURNAL OF DYNAMIC SYSTEMS, MEASUREMENT, AND CONTROL. Manuscript received March 14, 2005; final manuscript received September 16, 2005. Review conducted by Sunil A. Agrawal.

impedance-type FRVFs on a telemanipulator has added complexity because the system has more degrees of freedom, since there are two independent mechanical systems. The slave device can never be modeled perfectly, and information about the slave states are only obtained through quantized and sampled sensors, as opposed to a proxy, which is completely controlled in software.

In previous experiments [3], we found that implementing an impedance-type FRVF on the slave of a telemanipulator can lead to unwanted vibrations as the slave manipulator is pulled into the forbidden region by the master. These vibrations are not predicted by simple linear time-invariant (LTI) models and are most likely the manifestation of an unstable system, with nonlinearities that cause a limit cycle. Regardless of the reason, any sustained vibration is unwanted. Slave-side FRVFs are more difficult to stabilize than simple haptic virtual walls because the slave manipulator does not have the additional damping provided by the human operator. It may also be desirable to implement virtual fixtures on both the master and slave devices, simultaneously.

This paper considers a general system where the master and slave devices can each have FRVFs of different stiffness but at the same position (in their respective workspaces). We consider the underlying telemanipulation control architecture to have any combination of proportional-derivative (PD), velocity-feedback, and force-feed-forward control. We assume that we begin with an existing telemanipulation system that is designed to be well behaved for the desired MIS task and that we would like to overlay stable FRVFs on this system. We ask the question: "If a user attempts to apply a constant force to the master manipulandum of a bilateral telemanipulator, where the master and/or slave manipulator is interacting with a FRVF, will the system reach a static equilibrium or will it vibrate, and can this system behavior be predicted without simulating or physically implementing the system?" The results of this research indicate that these unwanted vibrations can be predicted given an accurate model of the master and slave devices and relatively simple bounds on human operator parameters.

There has been recent interest in FRVFs for telemanipulation assistance, but to the best of the authors' knowledge, this work represents the first control-theoretic analysis of the stability of these FRVFs. To accomplish the stability analysis, we make use of a set of observations and assumptions that are different from previous work in this field of research in several ways. First, preliminary experiments show that, when implementing a telemanipulation controller on a digital computer, the sampling rate of the system is very important in determining system stability (which should come as no surprise), but it is also significantly more important than other system nonlinearities (such as quantization from measuring position with optical encoders). Although many previous works consider pure time delays in the system, or frequency-domain approximations of the zero-order hold (ZOH), in this section we explicitly consider the sampling rate of the sampled-data system to accurately account for this important system parameter. Second, a human operator is often modeled as time varying, which is true, in general, but possibly unnecessary. Observations of malicious users attempting to drive haptic systems unstable indicate that the user adapts his or her hand properties until the perfect set of properties are found to make the system go unstable, but then the adaptation seems to stop, and the constant malicious user allows the limit cycle to continue. In this section, we consider a worst-case time-invariant human, which simplifies the analysis. Finally, many previous works model the human as passive, which, along with telemanipulator passivity, is a sufficient condition for system stability. In practice, when a human is attempting to act passively (i.e., not actively changing impedance properties), he or she is likely to behave dissipatively due to friction losses. In this paper, we account for the dissipation in the human user, resulting in a stability analysis that is potentially less conservative than one based on passivity methods.

2 System Model

We will adopt a system model similar to that of Lawrence [19]. The human is modeled with an LTI model

$$F_h^*(s) - F_h(s) = Z_h(s)X_m(s) \tag{1}$$

F_h is the human/master interaction force. F_h^* is defined as the exogenous human input; this does not represent an actual force in the system, but rather the input that acts to change the equilibrium point of the system. The assumption that position and force control in the human limb is achieved by simultaneously modifying the system's impedance and equilibrium point is known as equilibrium-point control [20]. F_h^* simply acts to change the coordinates of the system, without affecting the dynamic properties of the human. X_m is the position of the master device (which is equivalent to the position of the human when they are in contact), and X_s is the position of the slave. Without loss of generality, we assume $X_m = X_s$ represents perfect position tracking (a scaling factor could be included, but that does not affect our approach). The human impedance Z_h is modeled as an LTI mass-spring-damper system

$$Z_h(s) = m_h s^2 + b_h s + k_h \tag{2}$$

Modeling a human as a mass-spring damper is a fairly common approximation, and there is evidence that this is an accurate model over short time intervals [21]. The master and slave device dynamics are approximated by linear models

$$F_h(s) - F_{am}(s) = Z_m(s)X_m(s) \tag{3}$$

$$F_{as}(s) - F_e(s) = Z_s(s)X_s(s) \tag{4}$$

where Z_m and Z_s are the master and slave device impedances, respectively; F_{am} and F_{as} are the master and slave actuator forces, respectively; and F_e is any external environmental load on the slave. We will assume that the slave only interacts with passive environments. The master and slave impedances are modeled as LTI mass-damper systems

$$Z_m(s) = m_m s^2 + b_m s \tag{5}$$

$$Z_s(s) = m_s s^2 + b_s s \tag{6}$$

The impedances above are often written in terms of velocities V_m and V_s rather than positions X_m and X_s. This simply scales the impedances by a factor of s. Working in terms of velocity often simplifies the analysis of telemanipulator stability (since the multiplication of force and velocity defines an instantaneous power flow), but we consider positions here to explicitly keep track of the positions of the master and slave with respect to their FRVFs, and also to acknowledge that position is the quantity that is typically sensed and used in the digital controller.

Figure 1 shows the general telemanipulator system we consider; it is often referred to as a three-channel architecture. It is similar to that in [19], but we explicitly consider the discrete nature of the controller; continuous systems are written in s domain, and discrete systems are written in z domain. Each discrete control block $C(z)$ is preceded by a sampler and succeeded by a ZOH. The ZOHs result in actuator forces that are continuous-time staircase signals.

We implement a FRVF, at sample k, as a simple spring with a unilateral constraint

$$F_{iVF}(k) = \begin{cases} K_{iVF}X_i(k) & : \quad X_i(k) > 0 \\ 0 & : \quad X_i(k) \leqslant 0 \end{cases} \tag{7}$$

where K_{iVF} is the stiffness of the FRVF and $i = \{m, s\}$ for master and slave. The FRVF force is held constant over the sample by a ZOH. We assume, without loss of generality, that the FRVF is located at $X_m = X_s = 0$, since the underlying telemanipulator behavior will be independent of the zero position.

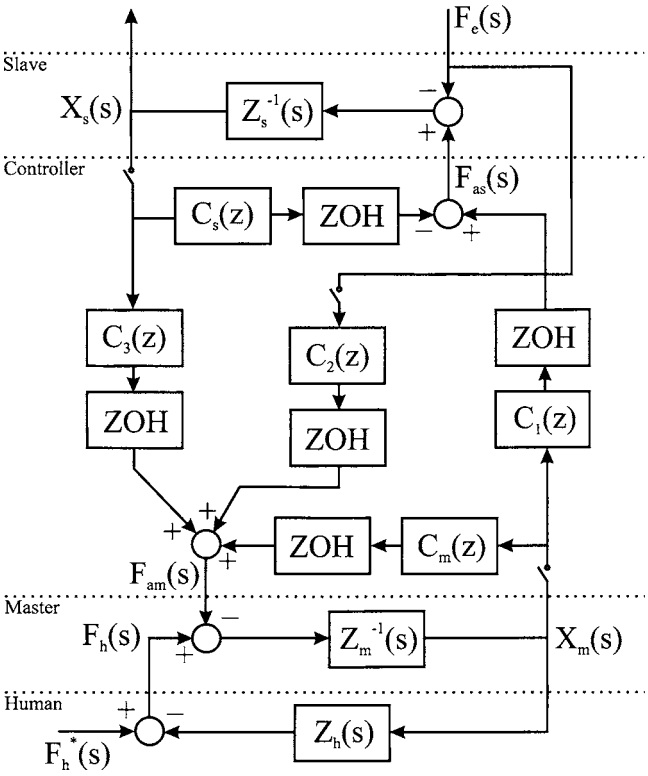

Fig. 1 General three-channel telemanipulator implemented with a digital computer

We consider the general class of telemanipulation control architectures that can be described by the equations (in time domain)

$$F_{am} = K_{pm}(X_m - X_s) + K_{dm}(\dot{X}_m - \dot{X}_s) + K_{vm}\dot{X}_m + K_{fm}F_e + F_{mVF} \tag{8}$$

$$F_{as} = K_{ps}(X_m - X_s) + K_{ds}(\dot{X}_m - \dot{X}_s) - K_{vs}\dot{X}_s - F_{sVF} \tag{9}$$

where K_{pm} and K_{ps} are the position gains of the master and slave, K_{dm} and K_{ds} are the derivative gains of the master and slave, K_{vm} and K_{vs} are additional velocity feedback gains of the master and slave, and K_{fm} is the force-feed-forward gain. This general class includes many common telemanipulation control architectures (summarized in [2,3]). We will only explicitly discuss this class of controllers, but the methods presented in this section could be applied to other control architectures as well.

The unilateral constraints of the FRVFs make even the continuous-time idealization of the control blocks C_m and C_s nonlinear—this motivates the equilibrium stability analysis of Sec. 3. This is followed by a discrete-time implementation of the idealized continuous-time controller.

3 Equilibrium Stability Analysis

When a slave device interacts with a stable impedance-type FRVF, the slave continues to move forward if the master moves forward, establishing an equilibrium point that balances the effects of the telemanipulation control system, the FRVF, and any external loads. Experiments show that when the slave device vibrates due to an unstable FRVF (that is, one that generates a limit cycle), the center of the vibration moves forward if the master moves forward, as seen in Fig. 2. Note that it is possible to generate vibrations that exist entirely within the forbidden region. This is evidence that the vibrations occur not on the surface of the FRVF, but rather, around an unstable equilibrium below the surface of the FRVF (as was observed in [22]). This phenomenon is also present when a master device vibrates against an unstable FRVF, though it is not as easy to observe.

In [2], we found that slave-side FRVFs are most effective at rejecting slave-side disturbances while minimizing position errors between the master and slave, which help maintain a sense of telepresence for the user. We also found that master-side FRVFs are most effective at rejecting disturbances on the master side (i.e., when the user attempts to command the slave into the forbidden region) while minimizing position errors between the master and slave. Preliminary experiments show that slave-side FRVFs tend to become unstable at much lower stiffness values than those on the master side (due to human damping on the master side). However, the observations above motivate the possible need for both slave- and master-side FRVFs in MIS tasks.

The unilateral constraint of the FRVF represents a significant nonlinearity in the system, and techniques based on hybrid system theory could be used to analyze the unilateral constraint of the FRVF. However, behavior such as that in Fig. 2 leads us to believe that other tools could be used to effectively predict instability. It appears that instability results from a divergence from an unstable equilibrium (note the beginnings of the instability in Fig. 2). We hypothesize that analysis of the equilibrium associated with a constant F_h^* will provide accurate results using relatively simple techniques. Also, we would not like to consider a limit cycle as a stable mode for our system when interacting with a FRVF; thus, equilibrium-point stability is a natural choice for a characterization of FRVF stability that corresponds to our intuition of well-behaved systems.

Preliminary experiments show that the condition when instabilities are most likely to occur is when the slave is in free space (i.e., $F_e=0$). Any contact of the slave with an environment only seems to destroy potential limit cycles. This even includes the case when the slave vibrates against a rigid environment. From an energy standpoint, each of these collisions is likely to provide a net dissipation. One can imagine a pathological case where a malicious exogenous F_e is perfectly constructed to create a limit cycle, but we assume here that the telemanipulator will only be interacting with passive environments. In addition, we are interested in applying FRVFs that are significantly stiffer than the relatively soft environments in MIS tasks. For these reasons, we will explicitly study the stability of the system when $F_e=0$.

3.1 Equilibrium Dual System. We consider the case where the human operator is trying to apply a constant positive force $\bar{F}_h$ to the master manipulandum; this is accomplished with a constant F_h^*. The actual force felt between the human and master will be a function of the feedback system and will deviate from the desired force by $\hat{F}_h$

$$F_h(t) = \bar{F}_h + \hat{F}_h(t) \tag{10}$$

Let $\bar{X}_m$ and $\bar{X}_s$ be the equilibrium positions of the system. They will be defined by the relationships

$$X_m(t) = \bar{X}_m + \hat{X}_m(t) \tag{11}$$

$$X_s(t) = \bar{X}_s + \hat{X}_s(t) \tag{12}$$

and will be functions of $\bar{F}_h$ and the control system gains. It is easy to verify that a unique equilibrium point exists, given any human impedance and F_h^*, by combining Eqs. (3)–(12) and then evaluating at the steady state. At the equilibrium position, the master and slave devices are in static-force equilibrium governed by the equations

$$\bar{F}_h + K_{pm}(\bar{X}_s - \bar{X}_m) = K_{mVF}\bar{X}_m \tag{13}$$

$$K_{ps}(\bar{X}_m - \bar{X}_s) = K_{sVF}\bar{X}_s \tag{14}$$

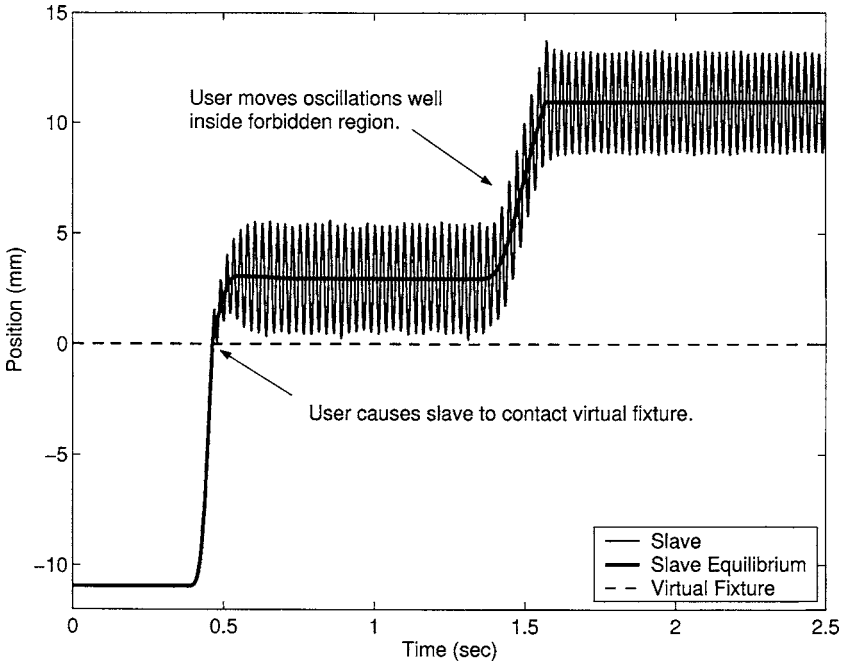

Fig. 2 Experimental data showing slave manipulator interacting with an unstable FRVF. The equilibrium position, based on the master position and the system gains, is also shown. Vibrations do not occur on the surface of the FRVF, but rather, around an unstable equilibrium. The system shown has K_{ps}=600 N/m, K_{vs}=2 Ns/m, K_{sVF}=3000 N/m, and all other gains are zero. The controller runs at 500 Hz.

We would like to analyze the stability of the system around the equilibrium point associated with a given $\bar{F}_h$. By substituting Eqs. (10)–(14) into the original system equations of Sec. 2, and making use of the fact that Z_m and Z_s are mass-damper systems with no spring terms (which results in $F_h=F_{am}$ and $F_{as}=0$ at equilibrium), the system can be rewritten as

$$Z_h(s)\hat{X}_m(s) = -\hat{F}_h(s) \tag{15}$$

$$Z_m(s)\hat{X}_m(s) = \hat{F}_h(s) - \hat{F}_{am}(s) \tag{16}$$

$$Z_s(s)\hat{X}_s(s) = \hat{F}_{as}(s) \tag{17}$$

where

$$\hat{F}_{am}(s) = (K_{pm} + K_{mVF})\hat{X}_m(s) - K_{pm}\hat{X}_s(s) + K_{dm}s[\hat{X}_m(s) - \hat{X}_s(s)] + K_{vm}s\hat{X}_m(s) \tag{18}$$

$$\hat{F}_{as}(s) = K_{ps}\hat{X}_m(s) - (K_{ps} + K_{sVF})\hat{X}_s(s) - K_{ds}s[\hat{X}_m(s) - \hat{X}_s(s)] + K_{vs}s\hat{X}_s(s) \tag{19}$$

Equations (15)–(19) represent a dual system to the one introduced in Sec. 2. The dual system is written in terms of positions and forces around the equilibrium, and the master and slave FRVFs are lumped with local master and slave controllers.

By considering the system in this way, there is a neighborhood around the equilibrium where the unilateral constraint of the FRVF is nonexistent (the size of the neighborhood has a "radius" of $\bar{X}_s$ on the slave side, and $\bar{X}_m$ on the master side); thus, for small deviations away from the equilibrium, the system will appear linear. Because this dual system, which includes virtual fixtures, can be written as a linear system around an equilibrium position, the stability of this equilibrium can be analyzed using a relatively simple technique—analysis of the system eigenvalues. Note that this dual system has no exogenous force inputs (compare Eqs. (15) and (17) to Eqs. (1) and (4), respectively). A constant exogenous force F_h^* influences the equilibrium position, but not the behavior around that equilibrium.

To analyze the stability of the above system, in Sec. 3.2, we create a linear state-space model of the system of Sec. 2 that does not include any unilateral constraints, but instead allows for the FRVFs to be included as in Eqs. (18) and (19).

3.2 Discrete State-Space Model. In this section, we develop a discrete state-space representation of the original system introduced in Sec. 2. The state-space model will consider the control system of Eqs. (8) and (9), without explicit consideration of the virtual fixtures. In Sec. 3.1, we established that analyzing the stability of this system will reveal stability information about the system that includes FRVFs.

We assume that no sensor is available to measure velocity directly, so the control system will use a backward-difference method to compute velocity

$$\dot{X}_m(k) = \frac{X_m(k) - X_m(k-1)}{T} \tag{20}$$

where T is the sampling period of the computer. $\dot{X}_s(k)$ is computed in the same way. Including this backward-difference in the state-space model is not an approximation if it is actually the way the controller measures velocity, which is common in practice. The individual control blocks are

$$C_1(z) = \frac{K_{ds}}{T}(1 - z^{-1}) + K_{ps1} \tag{21}$$

$$C_2(z) = K_{fm} \tag{22}$$

$$C_3(z) = -\frac{K_{dm}}{T}(1 - z^{-1}) - K_{pm3} \tag{23}$$

$$C_m(z) = \frac{K_{dm} + K_{vm}}{T}(1 - z^{-1}) + K_{pmm} \tag{24}$$

$$C_s(z) = \frac{K_{ds} + K_{vs}}{T}(1 - z^{-1}) + K_{pss} \tag{25}$$

Using a structure of this form will allow us to incorporate virtual fixtures into the state-space model, by setting $K_{pm3}=K_{pm}$ and $K_{pmm}=K_{pm}+K_{mVF}$, and by setting $K_{ps1}=K_{ps}$ and $K_{pss}=K_{ps}+K_{sVF}$.

In creating a discrete state-space model, we first find a discrete model for the continuous subsystems. By combining Eqs. (1) and (3), we get

$$F_h^*(s) - F_{am}(s) = Z_{hm}(s)X_m(s) \tag{26}$$

where $Z_{hm}(s)=Z_h(s)+Z_m(s)$. F_{am} is the master actuator force being generated by the controller, which is held constant between samples with a ZOH. We assume that F_h^* varies slowly relative to the sampling frequency and can be modeled as constant over a sampling period. This is a reasonable assumption since F_h^* represents voluntary human action, which is very slow relative to computer speeds [23]. Because the force input of this subsystem can be considered constant throughout the sampling period, the discrete transfer function from force to position can be found using

$$Z_{hm}^{-1}(z) = (1 - z^{-1})\mathcal{Z}\left[\frac{Z_{hm}^{-1}(s)}{s}\right] \tag{27}$$

where $\mathcal{Z}[\mathcal{Y}(s)]$ is the z transform of the time series represented by the Laplace transform $\mathcal{Y}(s)$ [24]. This transfer function is exact at the samples. The transfer function $Z_s^{-1}(z)$ is calculated in an analogous way from Eq. (4). This assumes that F_e can be modeled as constant between samples, which will be reasonable if the sampling rate of the system is fast and the environment that the system interacts with is compliant, which should be the case for MIS tasks. This assumption is discussed further in Sec. 5. The z transforms of transfer functions of the form of Eqs. (2) and (6) can be found precomputed in [24].

Using the modeling assumptions above, we developed an LTI discrete state-space model

$$\mathbf{x}(k+1) = \mathbf{A}\mathbf{x}(k) + \mathbf{B}\mathbf{u}(k) \tag{28}$$

where the state vector and input vector of the system are given by

$$\mathbf{x}(k) = \begin{bmatrix} X_m(k) \\ X_m(k-1) \\ X_m(k-2) \\ X_s(k) \\ X_s(k-1) \\ X_s(k-2) \\ F_h^*(k-1) \\ F_e(k-1) \end{bmatrix}, \quad \mathbf{u}(k) = \begin{bmatrix} F_h^*(k) \\ F_e(k) \end{bmatrix} \tag{29}$$

The algorithm for numerically generating this model is given in [2]. This discrete state-space model was designed as a discrete system from the beginning and is not simply a discrete-time approximation of a continuous-time state-space model. The model has eight eigenvalues, but two of them are identically equal to zero in the z plane, due to the structure of the $\mathbf{A}$ matrix. The location of the remaining eigenvalues reveal stability and transient properties of the system. Any eigenvalue lying outside the unit circle in the z plane would indicate an unstable equilibrium [24]. If an equilibrium is deemed stable, characteristics of eigenvalues in the z plane are related to those in the s plane by

$$z = e^{sT} \tag{30}$$

We use the fact that for eigenvalues in the s plane, the damping ratio is found by

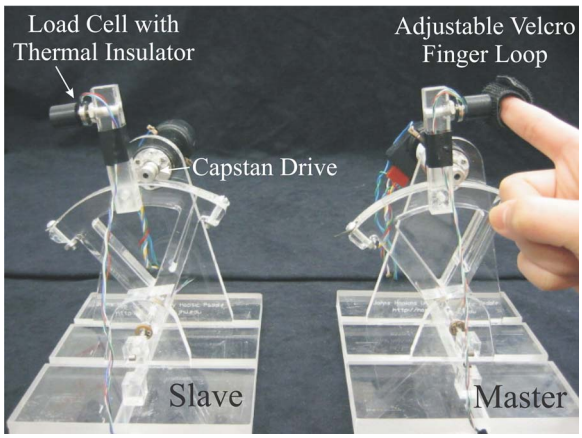

Fig. 3 Experimental 1-DOF impedance-type bilateral telemanipulation system based on modified haptic paddles

$$\zeta = \sin\left[\tan^{-1}\left(\frac{-\mathbb{R}\{s\}}{|\mathbb{I}\{s\}|}\right)\right] \tag{31}$$

The term "damping ratio" is only explicitly defined for second-order systems, but we apply the term analogously here to quantify the relationship between decay and oscillation in the components of the system's time response. By using knowledge of damping, we can require a more stringent condition than stability on our system; we can limit the magnitude and duration of decaying oscillations in the stable system. This leads to a more informative analytical result than passivity analysis.

4 Experimental Validation

In this section, we validate our proposed method on a real system that contains many unmodeled effects (quantization, unmodeled friction, actuator bandwidth and saturation, and unmodeled dynamics) and show that the proposed method is a good predictor of stability in real, nonideal systems.

Because the real system measures a quantized position signal, obtaining a velocity through a backward difference results in a noisy velocity signal. To mitigate this effect, a digital first-order low-pass filter with a bandwidth of 200 Hz is used to smooth the velocity measurement before it is used by the control system. Neither the quantization of the encoders nor this filter is included in the state-space model, but the experimental results show that the method is robust to these small unmodeled effects.

4.1 Telemanipulator. We have constructed a one-degree-of-freedom (1-DOF) bilateral telemanipulator based on a haptic device known as the haptic paddle [25]. The master and slave haptic paddles are geometrically identical, with a paddle rotation of 1 rad corresponding to a motion at the load cell with an arclength of 115 mm. The haptic paddles considered here have been modified from their original design [25] with Maxon dc motors (model 118754) with 500-count-per-turn Hewlett-Packard encoders. We have also added Entran ±10-N load cells (model ELFS-T3E-10N) to measure the applied user and environment forces. Delrin caps were added to thermally insulate each load cell. The telemanipulation system is shown in Fig. 3. The device properties are typical of haptic displays (back drivable, low friction, low inertia, low backlash). We use the PCI-DAS6402 data acquisition card from Measurement Computing Inc. to output voltages to the motor amplifiers and to input voltages from the load cells. The 16-bit D/A is configured for ±10 V, and the 16-bit A/D is configured for ±1.25 V. The output of the D/A is passed through current amplifiers that give a current through the motor that is proportional to the D/A voltage (i=0.33v); the current amplifiers are built around the National Semiconductor LM675 power op-amp. This gives us

direct control of applied torque on the motor. The resulting system has a force felt at the driving point that is proportional to the output voltage (1.65 N/V) statically. The signal from the load cells are passed through instrumentation amplifiers (Burr-Brown INA103) with a gain of five before they are read by the A/D. We use the PCI-Quad04, also from Measurement Computing, to interface with the encoders. A Velcro® finger loop is included on the master device, similar to those found on the daVinci™ Surgical System [14]. More details on the experimental system can be found in [2].

We begin by modeling our telemanipulator master and slave as masses with viscous friction. The haptic paddle is a rotational system, but we can find the equivalent linear system felt at the load cell as it moves along an arc. At every instant in time, the unactuated device should follow

$$m\ddot{x}(t) = F_h(t) - b\dot{x}(t) \tag{32}$$

where m is the effective mass of the device (in kilograms), b is the effective damping in the device Newton-seconds per meter, x is the position of the device along the arc (in meters), and F_h is the externally applied force along the arc (in newtons). By sampling the system at many instances, we may construct the matrix equation

$$[\ddot{\mathbf{x}}\ \dot{\mathbf{x}}][m\ b]^T = \mathbf{F_h} \tag{33}$$

This system can be written compactly with a data matrix **D** and a parameter vector **p**

$$\mathbf{Dp} = \mathbf{F_h} \tag{34}$$

The best estimate of the parameter vector, in a least-squares sense, is found using a pseudoinverse based on the singular value decomposition of **D** [26] (also known as the Moore-Penrose generalized inverse [27])

$$\mathbf{p} = \mathbf{D}^{\dagger}\mathbf{F_h} \tag{35}$$

To construct the **D** matrix, we "randomly" forced the device while holding the Velcro finger loop on the load cell, mitigating the effect of torques on the load cell (the Velcro finger loop was attached to the slave device as well for modeling purposes). Four runs of data were taken, with the load cell unloaded and recalibrated between each run—this was done to mitigate the effects of drift in the force measurement. Position and force data were recorded at each sample, and the position data was then used to construct the velocity and acceleration data. Because of the staircase discontinuous position measurement, the position data was smoothed off-line using a multiple-pass three-point moving-average filter [28] before differentiation. The velocity data was also smoothed before differentiation. The data sets were finally stacked to create the **D** matrix and the $\mathbf{F_h}$ vector, with a total of nearly 100,000 samples.

The resulting best-fit parameters are m_m=0.035 kg and b_m =0.41 Ns/m (r^2=0.92), and m_s=0.034 kg and b_s=0.49 Ns/m (r^2=0.91), indicating a good fit of the model [29]. The damping parameters indicate the actual differences in these devices that were designed to be identical. The mass and friction values given above are for the devices without the Delrin cap or Velcro finger loop (note the location of the Delrin cap with respect to the load cell). Once the Delrin caps are included, and the Velcro finger loop is included on the master, the resulting masses are m_m =0.040 kg and m_s=0.036 kg. The distribution of the data indicated that the r^2 metric is appropriate as a measure of how well the model fits the data.

4.2 Human Users. It is well known that the properties of the human user are important in determining the stability of bilateral telemanipulators [30]. For our method, we are interested in obtaining a worst-case LTI mass-spring-damper model of the human index finger (where the worst case is that which is most likely to make the system unstable). Rather than obtain new data that are specific to our system and human users, we chose to use previous data acquired by Hajian and Howe [21]. Figure 4 shows finger impedance data for five users. The data were taken at varying nominal force levels (corresponding to $\bar{F}_h$ in this paper). We have modified the plot by adding simple bounding lines, which are meant to represent possible worst-case user parameters at each force level. We note that Hajian and Howe make no claim about these five subjects being fully representative of the population as a whole or about the model's validity when $\bar{F}_h < 2$ N.

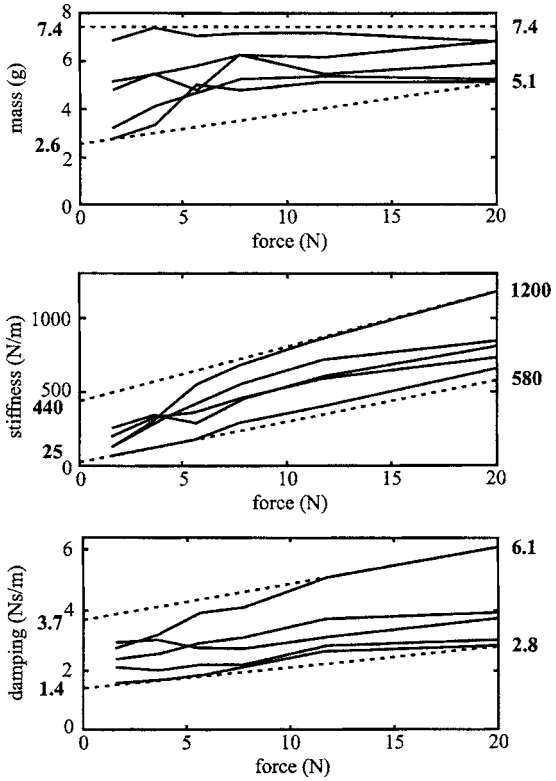

Fig. 4 Human-index-finger mass-spring-damper values for five users [21], with simple bounding lines added (original data courtesy Robert D. Howe)

Two human users were used to verify the method presented here. One user was large (100 kg, 1.91 m tall) and one user was small (49 kg, 1.55 m tall). These two users have index fingers with distinct mechanical properties (length, mass, strength); they were chosen to demonstrate the physical diversity that is possible between users that may possibly interact with the system. Both users were very experienced with the use of haptic devices.

For the experimental data that follow, the users attempted to make the system go unstable in any way possible, such that the index finger was through the Velcro finger loop and the elbow was resting. The goal was to determine the maximum FRVF stiffness at which he or she was unable to make the system go unstable (that is, generate a sustained limit cycle). For the purpose of this paper, a limit cycle that simply switched back and forth between two neighboring encoder counts was not considered unstable. This type of limit cycle may make the wall feel active (see [17,31]), but does not necessarily result in the gross instability that we are concerned with here.

Humans are adept at learning how to drive haptic systems to instability [16], and our users had as much time as necessary to experiment with the system, slowly lowering the FRVF stiffness level, until they were confident that they could not drive the system unstable. Many different strategies were learned and adopted, such as pushing hard, pushing softly, relaxing the hand, clenching the hand, fast movement into the FRVF, holding the device at the

```
input telemanipulator parameters
input human bounding model
for each user force level
   for each user mass at force level
      for each user damping at force level
         for each user stiffness at force level
            generate discrete state-space model
            convert eigenvalues to s-plane
            find minimum damping ratio ζ
            if current ζ < lowest ζ
               lowest ζ = current ζ
               worst-case user = current user
               worst-case force = current force
return lowest ζ
return worst-case user parameters
return worst-case force
if lowest ζ < 0
   return "system is unstable"
```

Fig. 5 Algorithm for determining system stability

surface of FRVF, and impulsively disturbing the slave. The users were also allowed to iterate, raising and lowering the FRVF stiffness as many times as was necessary to determine the limits of stability.

4.3 Algorithm. The algorithm used to determine if a possible instability exists is given in Fig. 5. It generates an LTI human by using the simple bounding lines from Fig. 4; at each force level, it creates many possible combinations of m_h, b_h, and k_h that could exist between the upper and lower bounding lines at that force level. This process is repeated for many possible force levels. For each LTI human user, the discrete state-space model is generated and the eigenvalues are analyzed. Rather than simply returning if the eigenvalues are stable ($|z|<1$ or $\mathbb{R}\{s\}<0$), the damping ratios of the eigenvalues are returned, as previously discussed, to give more information about the system's transient behavior.

Figure 6 shows the result of this algorithm run at two different values of K_{sVF}, with all other system parameters constant. The results of the two runs were superimposed to create the figure, and arrows were added to show how the clouds of eigenvalues (continuously) move as K_{sVF} is increased. Each cloud of eigenvalues was generated from 512 different human users that could exist between the bounding lines in Fig. 4 and shows how the system eigenvalues could vary based on the human user for a given system.

We now proceed by comparing the results predicted by the discrete state-space model to those actually observed in our real system. Because the possible combinations of controller gains are limitless, for the remainder of this section we limit our discussion to symmetric position-position telemanipulation controllers (except where noted). That is, $K_{pm}=K_{ps}\equiv K_p$, $K_{dm}=K_{ds}\equiv K_d$, $K_{vm}=K_{vs}=0$, and $K_{fm}=0$.

4.4 Slave FRVF Results. We first consider the FRVF on the slave side. Figure 7 shows the effect of sampling rate on the maximum stable FRVF that can be implemented on a typical telemanipulator. The experimental data were collected as described in the previous discussion of the human users. As is expected, the stiffness of the FRVF goes up with sampling rate. This figure indicates that the discrete state-space model is a good predictor of experimental data across sampling rates. It also appears that the stability of the slave FRVF is independent of the user; that is, both users were able to generate the finger properties necessary to maintain a limit cycle for roughly the same set of FRVF stiffnesses.

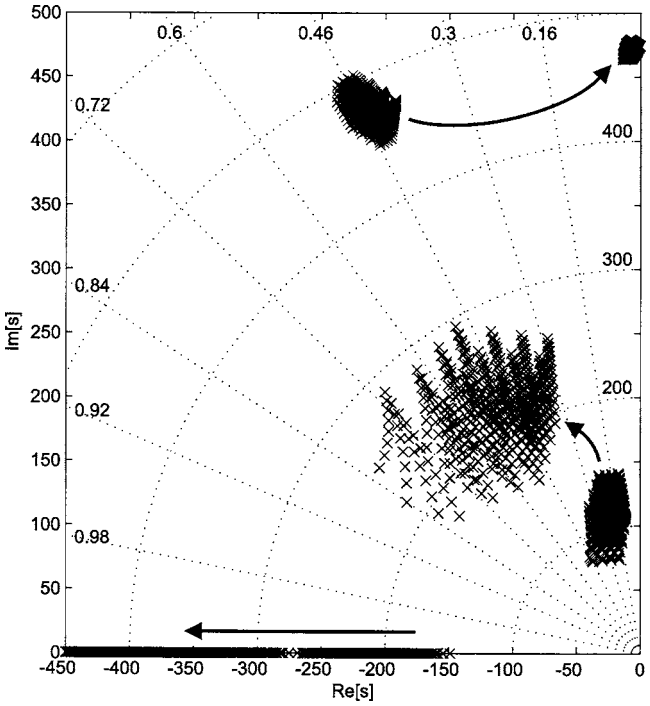

Fig. 6 The clouds of eigenvalues show how the system eigenvalues vary based on possible human users, for a system with $T=0.002$ s, $K_{pm}=K_{ps}=800$ N/m, and $K_{dm}=K_{ds}=6$ Ns/m. Arrows indicate how the eigenvalues move as the FRVF stiffness is increased from $K_{sVF}=500$ N/m to $K_{sVF}=5500$ N/m. Eventually, the eigenvalues reach the imaginary axis, indicating possible instability for the worst-case user.

We now look in more detail at the effects of the underlying telemanipulation controller gains on the stability of the FRVF. Figure 8 shows how the maximum stable slave FRVF changes as K_p and K_d are changed independently, for a system running at 500 Hz. These data show that K_p has a small effect on the stability, while K_d has a large effect. The small effect of K_p is likely because, for stable telemanipulators, the value of K_p is small relative to K_{sVF}. It is also again evident that there is little difference between users. Figure 9 shows the same type of plot for a system running at 1000 Hz. These data show the same trends, with an even better fit between the actual and the predicted stability.

A practical problem that must be addressed is saturation of the master actuators. In practice, the master device of a telemanipulation system may be designed to be light and back drivable, but a consequence of this design may be that the master actuators are small and saturate at relatively low force values. When the user applies enough force to saturate the master actuators, the actuators lose control authority and small changes in the system on the slave side lead to no changes in the master actuator's output, basically taking the master "out of the loop." We have found that this typically makes the slave device vibrate easier (that is, at a lower FRVF stiffness) than when the master is "in the loop;" thus, it is a problem that must be addressed.

To analyze saturation of the master actuators, we simply consider the system as a unilateral telemanipulator. The discrete state-space formulation is general enough to handle this case (using an equilibrium-point control model of the human results in the existence of an equilibrium point for a constant F_h^*, even when the master is completely unactuated). Figure 10 shows, across sampling rates, that the predictions match the observed data roughly as well as they did for the bilateral case. Of course, the user's properties have no effect on the performance of the unilateral system.

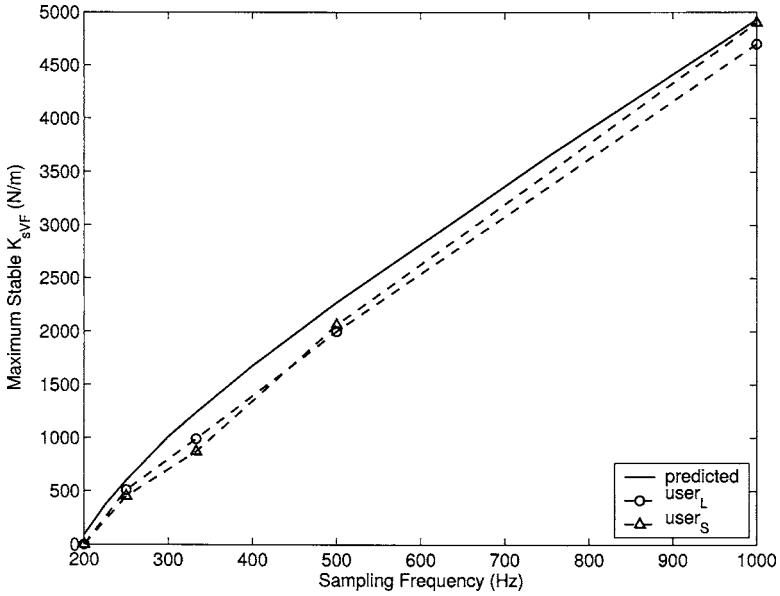

Fig. 7 Predicted and experimental stability bounds for slave FRVFs versus sampling rate, with K_p=600 N/m and K_d=2 Ns/m. Experimental data are shown for large (user$_L$) and small (user$_S$) users.

4.5 Master FRVF Results. We now consider the FRVF on the master side. Figure 11 shows the effect of sampling rate on the maximum stable FRVF that can be implemented on a typical telemanipulator. Again, as expected, the stiffness of the FRVF goes up with sampling rate. This figure shows significant differences from Fig. 7, though. First, there are significant differences between users, and the differences appear to grow as the sampling rate increases. The small user was able to generate finger impedances that the large user just could not, due to the inherent mechanical properties of the finger, making the system go unstable at lower stiffness values. Second, the prediction method appears to be conservative at high sampling rates.

To understand the effects of the underlying telemanipulator gains on FRVF stability, we first consider Fig. 12. This figure shows how the maximum stable FRVF changes as K_p and K_d are changed, independently, for a system running at 500 Hz. As before, the value of K_d has a large effect on the maximum FRVF stiffness, while the value of K_p has little effect. From this data, it is clear that the prediction is close to the data gathered for the small user, but is conservative for the large user. The fact that the prediction is conservative for one user and not for the other is exactly what would be expected if there is a discrepancy between

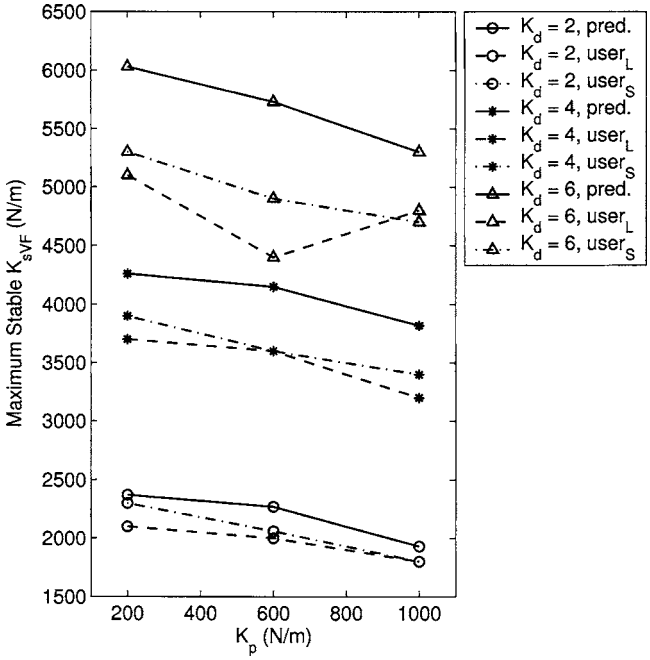

Fig. 8 Predicted and experimental stability bounds for slave FRVFs, at 500 Hz sampling rate. Data are shown for large (user$_L$) and small (user$_S$) users.

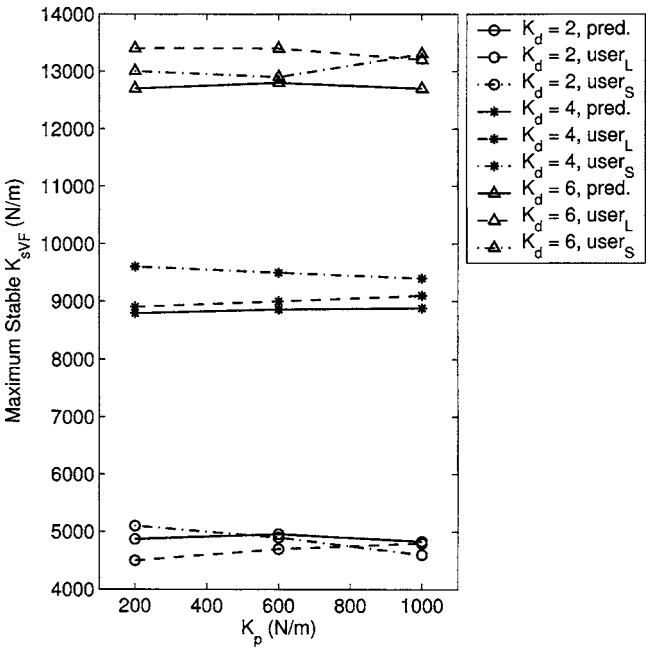

Fig. 9 Predicted and experimental stability bounds for slave FRVF, at 1000 Hz sampling rate. Data are shown for large (user$_L$) and small (user$_S$) users.

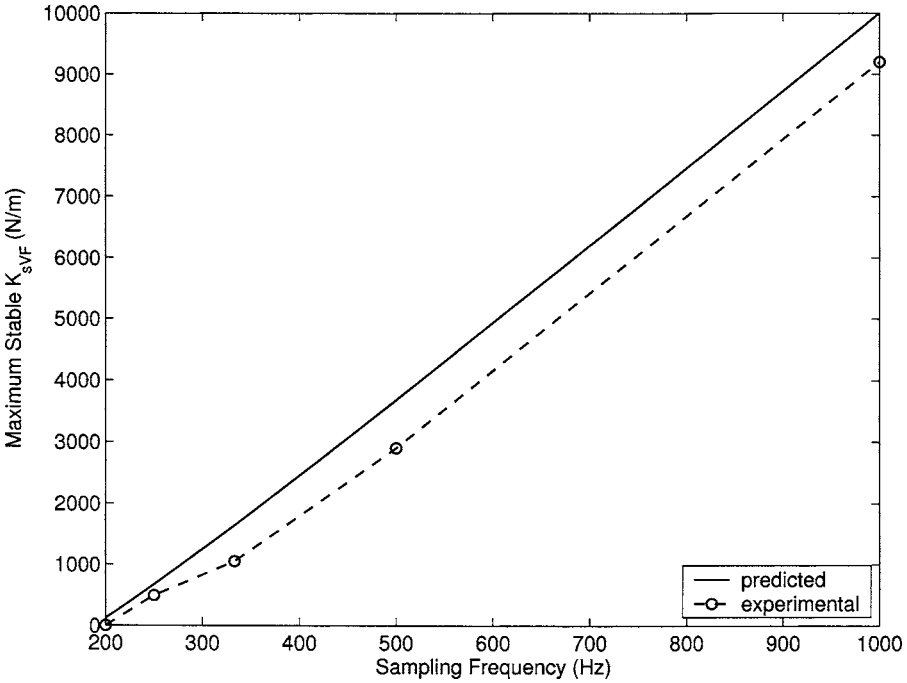

Fig. 10 Predicted and experimental stability bounds for slave FRVFs versus sampling rate for unilateral telemanipulation, with K_{ps}=1000 N/m and K_{ds}=6 Ns/m. A unilateral telemanipulator models saturation of the master actuator.

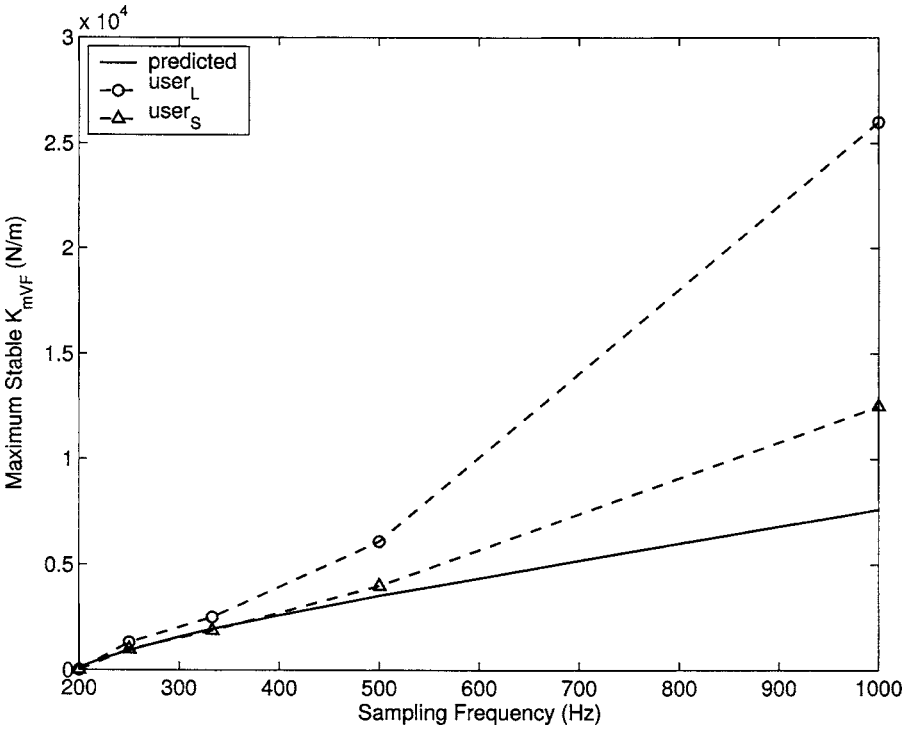

Fig. 11 Predicted and experimental stability bounds for master FRVFs versus sampling rate, with K_p=600 N/m and K_d=2 Ns/m. Experimental data are shown for large ($user_L$) and small ($user_S$) users.

users. The algorithm looks for the worst-case user, which in this case is a very small finger, and the prediction for all other users would necessarily be conservative.

Figure 13 shows the case where the sampling rate of the system has increased to 1000 Hz. For this case, the prediction is conservative for the small user and very conservative for the large user. In fact, the large user was never able to make the system go unstable in the same mode as the other instabilities presented in this section. For the large user, the FRVF stiffness was eventually turned up so high that the system went unstable due to the noise in the velocity signal, and not from the sampling rate. The instability felt different (very high frequency and low amplitude), and the figure indicates that the maximum stable FRVF stiffness actually decreases as K_d increases, which is expected for this type of

instability.

We now return to the case of the unilateral telemanipulator. A unilateral telemanipulator interacting with a master-side FRVF is essentially the same as a haptic device interacting with a virtual wall, since the slave manipulator has no effect on the master. Thus, this is an opportunity to directly compare our algorithm to previous work on virtual-wall stability. Figure 14 shows that, across sampling rates, our method is slightly conservative on the master side, but not nearly as conservative as requiring that our FRVF be passive (using a standard passivity result [32]). Recent work on virtual-wall passivity indicates that requiring passivity may be even more conservative, once position sensor quantization is considered [17,31].

5 Discussion

In Sec. 4 we showed that it is possible to accurately predict instabilities that result from telemanipulators interacting with stiff FRVFs, even though the closed-loop system contains an element as complex as a human. We obtained accurate predictions by explicitly considering sampling effects and showed that we need not consider the unilateral constraint of the FRVF explicitly. In addition, we showed that useful analytical results can be obtained with only rough LTI models of the human user. The experimental results of Sec. 4 demonstrate that our method is an effective tool in determining the limits on FRVF stiffness that can be safely implemented, without the need for extensive simulation in the design process. The method presented here is, in some sense, trial and error (choose system gains and then analyze system stability), but the system behavior and eigenvalue locations change in a way that should be expected (e.g., increasing position gains tends toward instability).

Our method explicitly considers a 1-DOF system, but the results are likely to translate to systems with higher degrees of freedom. Telemanipulators are typically implemented using Cartesian-based control (as opposed to direct joint control), and techniques such as the computed-torque method are available to decouple and linearize the Cartesian degrees of freedom [33]. With controllers such as this, the degree of freedom considered in our paper would simply correspond to the direction normal to the FRVF at the point of contact.

We explicitly considered the index finger of the human user here, but other system-appropriate human models could be used. For example, it has been shown that the human wrist can also be accurately modeled as LTI mass-spring-damper [34]. As a proof of concept, the idea that the human user can be modeled as a worst-case LTI model, rather than as a more general time-varying model, was shown to be accurate in predicting system stability bounds. In Sec. 4.2, we noted that Hajian and Howe [21] make no claim about the five subjects used in their experiment being fully representative of the population as a whole. It is possible that our experimental subjects lie outside of the bounding lines of Fig. 4. If a more complete data set were used, it could only increase the set of parameters used by the algorithm of Sec. 4.3, which, in turn, could only make the stability predictions more conservative.

It should be noted that actually implementing a FRVF stiffness just below the stability limit would probably not be desirable for real robot-assisted surgical tasks; sustained vibration may be impossible to generate, but a slowly decaying, large-amplitude vibration would be undesirable as well. A benefit of considering the location of the eigenvalues of the system as a measure of stability is that it is not a binary test, simply returning "stable" or "unstable." The damping in the eigenvalues can be used as an additional source of information about the system's transient response. In addition, the damping in the worst-case eigenvalue can be used as a rough measure of stability robustness (in second-order systems, the damping ratio is highly correlated to the phase margin in the system).

The method presented here was shown to be accurate in determining system stability when the slave is not in contact with any environment (which was determined to be the most likely scenario to result in sustained limit cycles). One assumption used in creating the discrete state-space model in Sec. 3.2 is the assumption that F_e is constant between samples. Our method was developed specifically for MIS applications, where the environment will be soft tissues with relatively low stiffness values. If the system in-

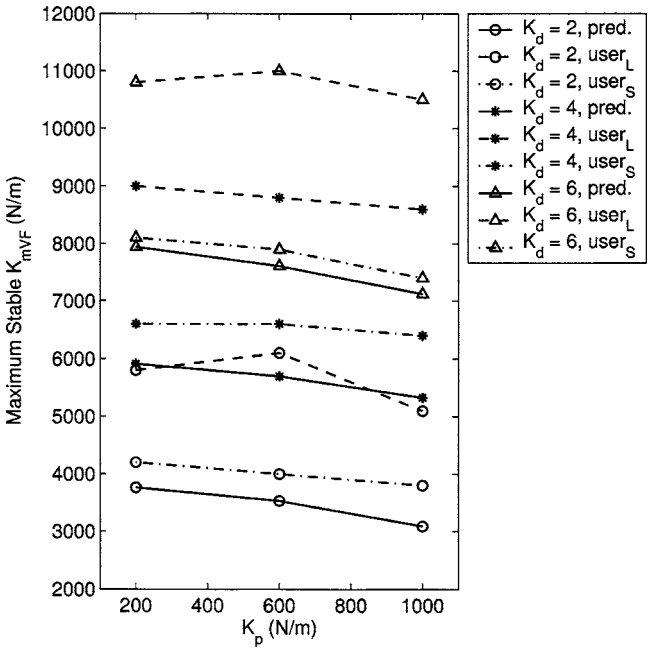

Fig. 12 Predicted and experimental stability bounds for master FRVFs, at 500 Hz sampling rate. Data are shown for large (user$_L$) and small (user$_S$) users.

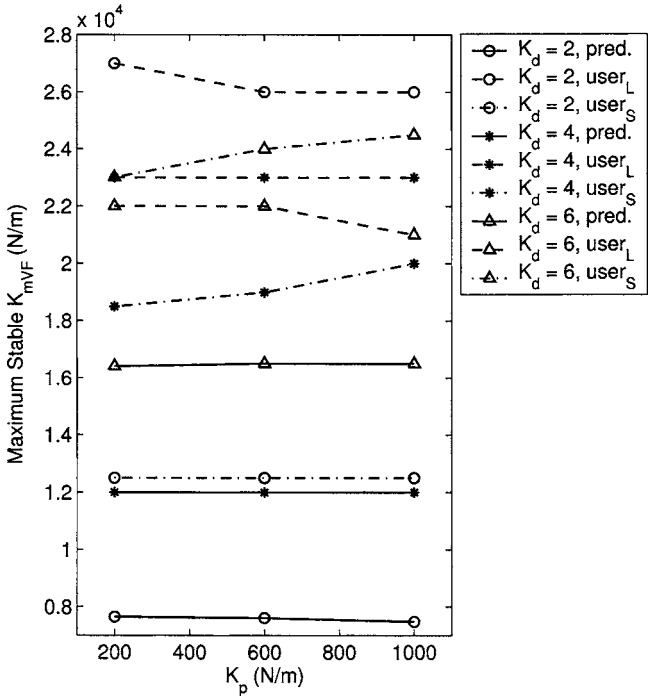

Fig. 13 Predicted and experimental stability bounds for master FRVFs, at 1000 Hz sampling rate. Data are shown for large (user$_L$) and small (user$_S$) users.

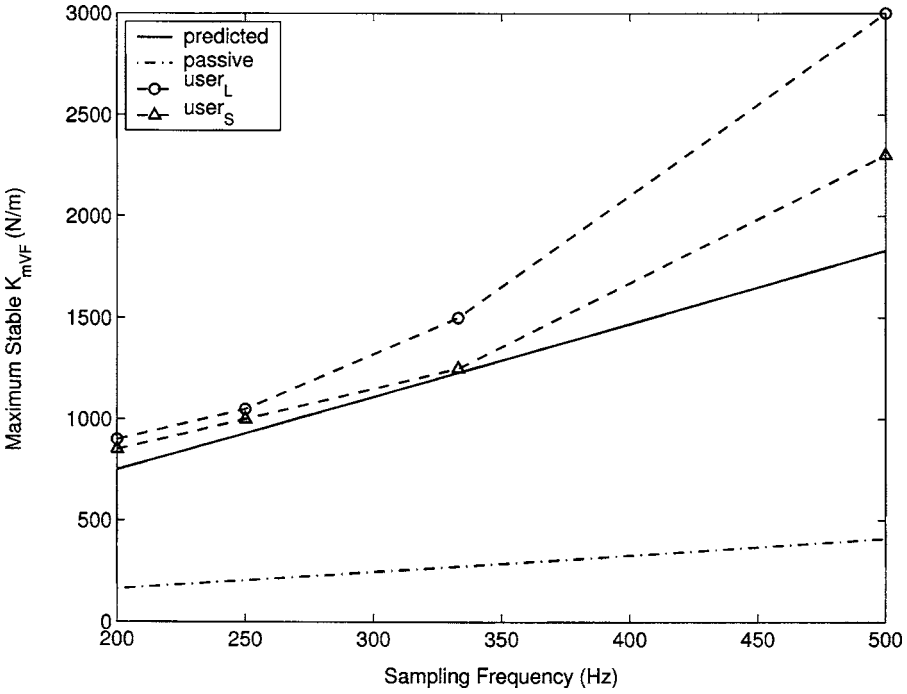

Fig. 14 Predicted and experimental stability bounds for master FRVFs versus sampling rate for unilateral telemanipulation, with K_{ps}=1000 N/m and K_{ds}=6 Ns/m (simple virtual wall). Experimental data are shown for large (user$_L$) and small (user$_S$) users. Requiring passivity of the FRVF gives a more conservative result.

teracts with stiff environments (relative to the sampling rate) where F_e could change significantly between samples, the model could lose accuracy. Verification of our method for systems where the FRVF is located at or below the surface of a compliant environment is left as a topic for future research, but preliminary experiments indicate that simply assuming no environment in the analysis will result in conservative stability predictions when a dissipative environment is present.

For completeness, let us briefly consider some of the limitations of our method. In particular, system models generally will have high-frequency inaccuracies and, as the models become less accurate, the analytical predictions will lose accuracy as well. The finger model loses accuracy at combinations of high sampling rate and high FRVF stiffness. The properties of the finger pad may be important here [35], but they are unmodeled in [21], which is the source for our finger data. The unmodeled effects of the finger pad are likely to make the finger more dissipative. Another possible inaccuracy is that the actuators (including their amplifiers) could deviate from the ideal actuator assumed in the model. Because of inductance in the motors and voltage limits in the current amplifiers, the actual rate of change in current through the motors is limited (although very fast) [2]. This effect would be most noted with high sampling rate and high FRVF stiffness, and it would tend to make the effective FRVF stiffness slightly lower than what is expected. Finally, for small movements, unmodeled friction (such as Coulomb friction) tends to dominate, and the viscous friction tends to underestimate the actual dissipation. All of the above effects would tend to make the method predict in a conservative (safe) way. However, our result was shown to be less conservative than that obtained using FRVF passivity as a sufficient condition for closed-loop stability, as shown in Fig. 14.

We also did not consider effects of mechanical compliance. Our experimental telemanipulator is very rigid, with the compliance occurring in the controlled joints. Consequently, we were able to accurately model our system as rigid bodies. This will not be the case with all systems; structural resonance is often an important limitation in robot design [33]. Structural dynamics could be incorporated into a state-space analysis, such as that presented here; this would increase the dimension of the model.

6 Conclusions

This work presents a method to predict and prevent unstable vibrations of the master and slave manipulators of a bilateral telemanipulation system against forbidden-region virtual fixtures (FRVFs), implemented as virtual walls, through appropriate choice of control system gains and FRVF stiffness. With an understanding of the bounds of their stability, FRVFs can be safely overlayed on existing bilateral telemanipulation systems. FRVFs can be applied to robot-assisted minimally invasive surgical procedures to prevent the manipulator from entering into forbidden regions of the workspace, preventing unwanted and potentially dangerous interactions with delicate tissues.

We found that a telemanipulator with FRVFs can be rewritten around an equilibrium position, creating a dual system that can be analyzed using methods already available for linear systems. Then we developed a discrete state-space model for a class of bilateral telemanipulators that includes many common telemanipulator control systems. The algorithm for generating this model is given in [2]. We then used the eigenvalues of this model to analyze the stability of the system. The eigenvalues also provide insight into transient response in the system, which is not available using some other stability methods (such as passivity).

Our method uses a worst-case LTI mass-spring-damper model of the human user (rather than a complicated nonlinear time-varying model or a general passive model) and a simple mass-damper model for the master and slave devices. However, it explicitly considers the sampling rate of the system. Experimental results show agreement with analytical predictions of stability in a real nonideal system. Results indicate that unwanted vibration of the slave manipulator against a slave-side FRVF is independent of the type of user (i.e., large or small hand), but is dependent on the

impedance properties adopted by the user. It was found that the type of user is important in generating sustained vibrations of the master manipulandum against a master-side FRVF. Our result was also shown to be less conservative than requiring passivity of a master FRVF.

Acknowledgment

The authors would like to thank Robert D. Howe for permission to reprint his finger data. The authors would also like to thank Panadda Marayong for her help collecting data. This material is based on work supported by the National Science Foundation, Grant Nos. ITR-0205318 and IIS-0347464.

References

[1] Sheridan, T. B., 1992, *Telerobotics, Automation, and Human Supervisory Control*. The MIT Press, Cambridge, MA.
[2] Abbott, J. J., 2005, "Virtual Fixtures for Bilateral Telemanipulation," Ph.D. dissertation, Department of Mechanical Engineering, The Johns Hopkins University.
[3] Abbott, J. J., and Okamura, A. M., 2003, "Virtual Fixture Architectures for Telemanipulation," *Proc. IEEE Int'l. Conf. on Robotics and Automation*, IEEE, New York, pp. 2798–2805.
[4] Abbott, J. J., and Okamura, A. M., 2003, "Steady-Hand Teleoperation With Virtual Fixtures," *Proc. of 12th IEEE Int'l. Workshop on Robot and Human Interactive Communication (RO-MAN)*, IEEE, New York, pp. 145–151.
[5] Bettini, A., Marayong, P., Lang, S., Okamura, A. M., and Hager, G. D., 2004, "Vision-Assisted Control for Manipulation Using Virtual Fixtures," IEEE Trans. Rob. Autom., **20**(6), pp. 953–966.
[6] Li, M., and Taylor, R. H., 2004, "Spatial Motion Constraints in Medical Robot Using Virtual Fixtures Generated by Anatomy," *Proc. of IEEE Int'l. Conf. on Robotics and Automation*, IEEE, New York, pp. 1270–1275.
[7] Moore, C. A., Peshkin, M. A., and Colgate, J. E., 2003, "Cobot Implementation of Virtual Paths and 3-D Virtual Surfaces," IEEE Trans. Rob. Autom., **19**(2), pp. 347–351.
[8] Park, S., Howe, R. D., and Torchiana, D. F., 2001, "Virtual Fixtures for Robotic Cardiac Surgery," *Proc. 4th Int'l. Conf. on Medical Image Computing and Computer-Assisted Intervention*, IEEE, New York, pp. 1419–1420.
[9] Payandeh, S., and Stanisic, Z., 2002, "On Application of Virtual Fixtures as an Aid for Telemanipulation and Training," *Proc. of 10th Symposium on Haptic Interfaces for Virtual Environments and Teleoperator Systems*, IEEE, New York, pp. 18–23.
[10] Rosenberg, L., 1993, "Virtual Fixtures: Perceptual Tools for Telerobotic Manipulation," *Proc. of IEEE Virtual Reality Int'l. Symposium*, IEEE, New York, pp. 76–82.
[11] Sayers, C., 1999, *Remote Control Robotics*. Springer-Verlag, Berlin.
[12] Turro, N., and Khatib, O., 2000, "Haptically Augmented Teleoperation," *Proc. of 7th Int'l. Symposium on Experimental Robotics*, Springer-Verlag, Berlin, pp. 1–10.
[13] Guthart, G. S., and Salisbury, J. K., 2000, "The Intuitive™ Telesurgery System: Overview and Application," *Proc. of IEEE Int'l. Conf. on Robotics and Automation*, IEEE, New York, pp. 618–621.
[14] Intuitive Surgical, http://www.intuitivesurgical.com.
[15] Wagner, C. R., Stylopoulos, N., and Howe, R. D., 2002, "The Role of Force Feedback in Surgery: Analysis of Blunt Dissection," *Proc. of 10th Symposium on Haptic Interfaces for Virtual Environments and Teleoperator Systems*, IEEE, New York, pp. 68–74.
[16] Colgate, J. E., and Brown, J. M., 1994, "Factors Affecting the Z-Width of a Haptic Display," *Proc. of IEEE Int'l. Conf. on Robotics and Automation*, IEEE, New York, pp. 3205–3210.
[17] Abbott, J. J., and Okamura, A. M., 2005, "Effects of Position Quantization and Sampling Rate on Virtual-Wall Passivity," IEEE Trans. Rob. Autom., **21**(5), pp. 952–964.
[18] Zilles, C. B., and Salisbury, J. K., 1995, "A Constraint-Based God-Object Method for Haptic Display," *Proc. of IEEE/RSJ Int'l. Conf. on Intelligent Robots and Systems*, IEEE, New York, pp. 146–151.
[19] Lawrence, D. A., 1993, "Stability and Transparency in Bilateral Teleoperation," IEEE Trans. Rob. Autom., **9**(5), pp. 624–637.
[20] Bizzl, E., Hogan, N., Mussa-Ivaldi, F. A., and Giszter, S., 1992, "Does the Nervous System Use Equilibrium-Point Control to Guide Single and Multiple Joint Movements?," Behav. Brain Sci., **15**, pp. 603–613.
[21] Hajian, A. Z., and Howe, R. D., 1997, "Identification of the Mechanical Impedance at the Human Finger Tip," ASME J. Biomech. Eng., **119**, pp. 109–114.
[22] Salcudean, S. E., and Vlaar, T. D., 1997, "On the Emulation of Stiff Walls and Static Friction With a Magnetically Levitated Input/Output Device," ASME J. Dyn. Syst., Meas., Control, **119**, pp. 127–132.
[23] Wickens, C. D., 2000, *Engineering Psychology and Human Performance*, Harper Collins, New York.
[24] Franklin, G. F., Powell, J. D., and Workman, M. L., *Digital Control of Dynamic Systems*, 2nd ed., Addison-Wesley, Reading, MA.
[25] Okamura, A. M., Richard, C., and Cutkosky, M. R., 2002, "Feeling is Believing: Using a Force-Feedback Joystick to Teach Dynamic Systems," J. Eng. Educ., **92**(3), pp. 345–349.
[26] Strang, G., 1988, *Linear Algebra and its Applications*, 3rd ed. Harcourt Brace Jovanovich, Ft. Worth.
[27] Horn, R., and Johnson, C. R., 1985, *Matrix Analysis*, Cambridge University Press, Cambridge, United Kingdom.
[28] Smith, S. W., 1997, *The Scientist and Engineer's Guide to Digital Signal Processing*, California Technical Publishing, San Diego.
[29] Kleinbaum, D. G., Kupper, L. L., Muller, K. E., and Nizam, A., *Applied Regression Analysis and Other Multivariable Methods*, 3rd ed. Duxbury Press, Pacific Cove, CA.
[30] Hannaford, B., and Anderson, R., 1988, "Experimental and Simulation Studies of Hard Contact in Force Reflecting Teleoperation," *Proc. of IEEE Int'l. Conf. on Robotics and Automation*, IEEE, New York, pp. 584–589.
[31] Diolaiti, N., Niemeyer, G., Barbagli, F., Salisbury, J. K., and Melchiorri, C., 2005, "The Effect of Quantization and Coulomb Friction on the Stability of Haptic Rendering," *Proc. of World Haptics Conf.*, IEEE, New York, pp. 237–246.
[32] Colgate, J. E., and Schenkel, G. G., 1997, "Passivity of a Class of Sampled-Data Systems: Application to Haptic Interfaces," J. Rob. Syst., **14**(1), pp. 37–47.
[33] Craig, J. J., 1989, *Introduction to Robotics: Mechanics and Control*, 2nd ed., Addison-Wesley, Reading, MA.
[34] Kuchenbecker, K. J., Park, J. G., and Niemeyer, G., 2003, "Characterizing the Human Wrist for Improved Haptic Interaction," *Proc. of ASME Int'l. Mechanical Engineering Congress and Exposition*, November, Washington, D.C., ASME, New York, pp. 1–8.
[35] Lundström, R., 1984, "Local Vibrations—Mechanical Impedance of the Human Hand's Glabrous Skin," J. Biomech., **17**(2), pp. 137–144.